ISSN: 0256-307X

中国物理快报

Chinese Physics Letters

Volume 34 Number 9 September 2017

A Series Journal of the Chinese Physical Society
Distributed by IOP Publishing

Online: http://iopscience.iop.org/0256-307X
http://cpl.iphy.ac.cn

CHINESE PHYSICAL SOCIETY
IOP Publishing

CHIN. PHYS. LETT. Vol. 34, No. 9 (2017) 094301

Geoacoustic Inversion Using Time Reversal of Ocean Noise *

Ji-Xing Qin(秦继兴)[1**], Boris Katsnelson[2], Oleg Godin[3], Zheng-Lin Li(李整林)[1]

[1]*State Key Laboratory of Acoustics, Institute of Acoustics, Chinese Academy of Sciences, Beijing 100190*
[2]*Department of Marine Geosciences, School of Marine Sciences, University of Haifa, Haifa 31905, Israel*
[3]*Cooperative Institute for Research in Environmental Sciences, University of Colorado Boulder, Colorado 80309, USA*

(Received 26 May 2017)

We present a passive geoacoustic inversion method using two hydrophones, which combines noise interferometry and time reversal mirror (TRM) techniques. Numerical simulations are firstly performed, in which strong focusing occurs in the vicinity of one hydrophone when Green's function (GF) is back-propagated from the other hydrophone, with the position and strength of the focus being sensitive to sound speed and density in the bottom. We next extract the GF from the noise cross-correlation function measured by two hydrophones with 8025-m distance in the Shallow Water '06 experiment. After realizing the TRM process, sound speed and density in the bottom are inverted by optimizing focusing of the back-propagated GF. The passive inversion method is inherently environmentally friendly and low-cost.

PACS: 43.30.Pc, 43.30.Ma, 43.30.Nb, 43.60.Tj DOI: 10.1088/0256-307X/34/9/094301

Wave propagation in oceans is usually influenced significantly by bottom properties, especially for shallow water or transitional areas. Due to the difficulty and high cost of direct measurement for the bottom parameters, geoacoustic inversion as an important kind of indirect method has received considerable attention in underwater acoustics. A variety of inversion methods have been developed in recent years,[1−8] and most of them are based on active schemes. In the active inversion methods, physical properties of the environment affecting acoustic propagation can be retrieved from observations of signals generated by powerful controlled sound sources.[9]

Passive acoustic inversion method employs the ubiquitous ambient noise as a replacement of the designated probing signals.[10] For the passive method, a critical issue is Green's function (GF) retrieval. The process by which approximations to GFs between two locations are estimated by cross-correlating time series of ambient noise recorded at those locations is widely referred to as noise interferometry (NI). The underlying theory has been well developed.[11−14]

It is well known that if a pulse signal is radiated at one point and the field is recorded at multiple distant locations, then retransmitting the time-reversed recorded signals at those locations results in a wave field that focuses at the original sound generation point.[15−17] This process is referred to as implementation of a time reversal mirror (TRM). Roux and Kuperman[18] firstly demonstrated that the GFs obtained from noise cross-correlation functions (NCCFs), rather than measured responses to active source transmissions, can be used to successfully implement a TRM. The time reversal of ocean noise makes one of the receivers act as a virtual source.

In this Letter, we combine the NI and TRM techniques to invert ocean bottom parameters passively. Firstly, numerical simulations are performed to verify that bottom parameters can be determined from the requirement that the TRM focuses the wave field at the position of the sound source or, by extension, of the virtual source created through NI. Secondly, we extract the GF from the NCCF measured by two single hydrophones in the Shallow Water '06 (SW06) experiment.[19] Thirdly, combined with the extracted GF, the TRM is used to search for the optimal sound speed and density in the bottom.

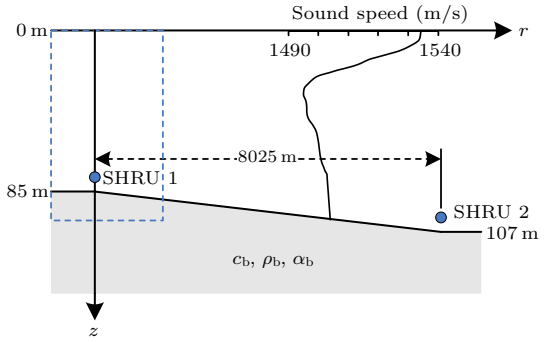

Fig. 1. Geometry of the ocean environment between SHRU 1 and SHRU 2 in the SW06 experiment.

We consider the ocean environment as shown in Fig. 1, which is the same as one part of the SW06 experiment. In the experiment, five single hydrophone receiving units (SHRUs) were positioned on the across shelf path. We choose the waveguide between SHRU 1 and SHRU 2 to analyze. The water depth at the position of SHRU 1 is 85 m, and that at the position of SHRU 2 is 107 m. We assume that the bathymetry between the two receivers varies linearly. Both of the SHRUs are located 7 m above the bottom, and the horizontal distance between them is 8025 m. The bottom is modeled as a uniform fluid halfspace in this work. The averaged sound speed profile measured in the experiment is used in the following simulations.

Let a point sound source be located at the position of SHRU 1, to emit a signal $s_0(t)$ with a spectrum

*Supported by the National Natural Science Foundation of China under Grant Nos 11434012 and 41561144006.
**Corresponding author. Email: qjx@mail.ioa.ac.cn

$S(\omega)$. The spectrum has the form

$$S(\omega) = \begin{cases} 1, & 10\,\text{Hz} \le \omega/2\pi \le 70\,\text{Hz}, \\ 0, & \text{elsewhere}. \end{cases} \quad (1)$$

In the frequency domain, the acoustic pressure at the position of SHRU 2 is given by

$$P(\boldsymbol{r}_2, \omega) = S(\omega)G(\omega), \quad (2)$$

where $G(\omega)$ is the frequency-domain GF between the points of SHRUs 1 and 2. Next, reverse the received time-domain signal and reradiate it. The acoustic pressure received at the position of SHRU 1 is

$$P(\boldsymbol{r}_1, \omega) = S^*(\omega)G^*(\omega)G(\omega), \quad (3)$$

where $*$ denotes the complex conjugation. The focusing field is expected at the point of SHRU 1 if there are sufficient multi-paths connecting the two points. We calculate the frequency-domain acoustic pressure $P(r, z, \omega)$ using a wide-angle parabolic equation model RAM.[20] Subsequently, time-domain pressure $p(r, z, t)$ is Fourier-synthesized from $P(r, z, \omega)$. We define $E(r, z) = |\max_{t>0}[p(r, z, t)]|^2$. The normalized peak intensity $J(r, z) = -10\lg[1 - 0.99E(r, z)/E_0]$, with $E_0 = \max_{r,z}[E(r, z)]$, is given in the dashed rectangular area around SHRU 1 as shown in Fig. 1 in the following results. Figure 2(a) shows the simulation result using the bottom parameters with the sound speed of 1750 m/s, the density of 1.9 g/cm^3, and the attenuation of 0.02 dB/wavelength. A sharpened focus can be observed in Fig. 2(a) exactly at the position of SHRU 1. If the bottom parameters for wave propagating from SHRU 1 to SHRU 2 are different from those for back-propagating, the main focus will shift and blur, or the spurious additional foci will become more pronounced. From Figs. 2(b)–2(d), we can see that the main-focus shift of the back-propagating wave is sensitive to mismatches of sound speed and density in the bottom. The simulation results suggest that bottom parameters can be estimated from the position of focusing sound field generated by the TRM. It should be emphasized that the focusing position is insensitive to the bottom attenuation coefficient, which is considered as a constant of 0.02 dB/wavelength in this study.

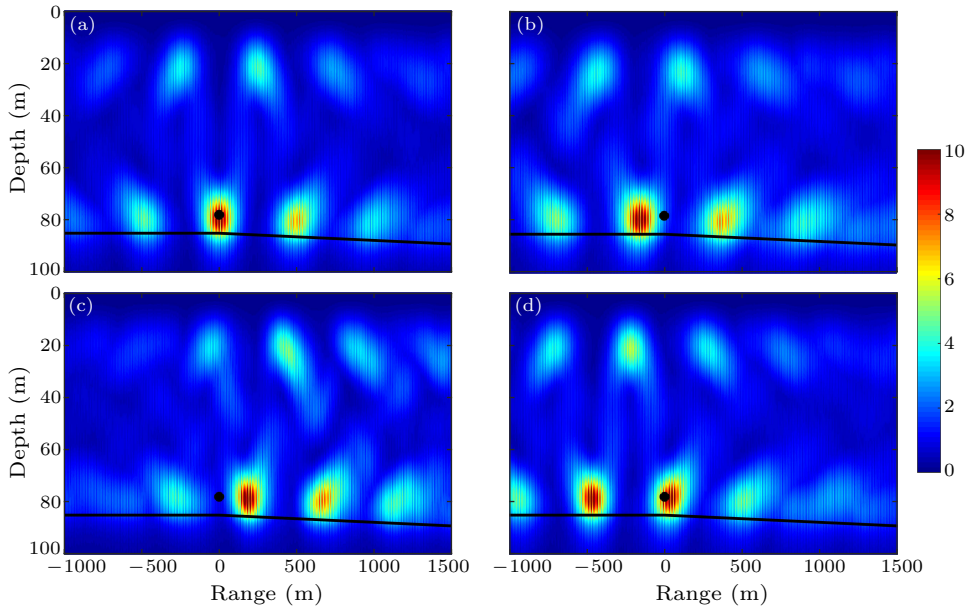

Fig. 2. Sensitivity for the position shift of focusing wave field generated by the TRM to the bottom parameters. The sound speed is 1750 m/s and the density is 1.9 g/cm^3 in the bottom for forward wave propagating. The sound speed and density for back-propagating are (a) 1750 m/s and 1.9 g/cm^3, (b) 1700 m/s and 1.9 g/cm^3, (c) 1850 m/s and 1.9 g/cm^3, and (d) 1750 m/s and 1.5 g/cm^3. In each panel, the black dot denotes the position of the sound source, and the bathymetry is indicated by a thick black line.

For noise data recorded by SHRUs 1 and 2 in the SW06 experiment, we evaluate the NCCF from a Fourier transform of the cross spectrum, which is calculated by summating over a large number of data segments in 5.7 d. There are 10% data segments with the highest noise level that are discarded to suppress contributions of strong, localized and transient sources. To equalize contributions of various sources, the noise spectra are normalized in each data segment. Figure 3(a) shows the final result in the frequency band of 10–70 Hz, in which there are two peaks around the time delays of ±5.5 s, respectively. The NCCF is approximately proportional to the sum of forward and backward GFs between SHRU 1 and SHRU 2, i.e., $C(t) = A[G(t) + G(-t)]$, where A is a constant. An unexpected smaller peak also appears in Fig. 3(a) because some signals are probably treated as noise. In the following we choose the negative time delay part of NCCF as GF, which is the waveform in the dashed box in Fig. 3(a). The fine structure of the backward GF is given in Fig. 3(b). In principle, we could obtain the same GF from the positive time delay part of

NCCF if the noise field is perfectly diffuse.

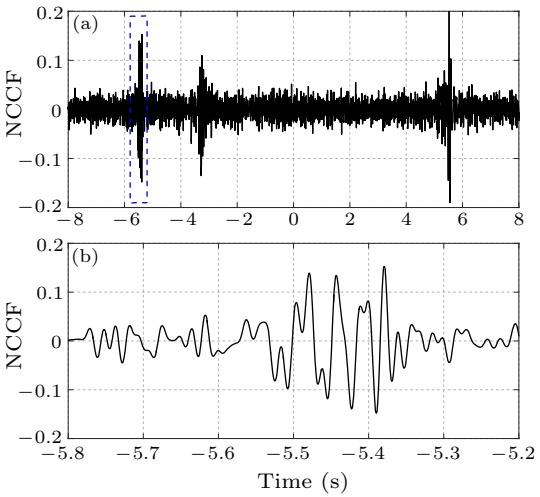

Fig. 3. The noise cross-correlation function (NCCF) for SHRUs 1 and 2 in the SW06 experiment (a) and the fine structure of negative time delay part (b). The frequency band is in the range of 10–70 Hz.

In the following we realize a passive TRM using the GF retrieved from the ambient noise to invert bottom parameters. The process of implementing TRM is almost the same as the above numerical simulations. The only difference is the absence of a source in the waveguide. Instead, SHRU 1 serves as a virtual source. At the position of SHRU 2, the retrieved GF is firstly time-reversed, then we reradiate the reversed signal and make it propagate toward SHRU 1 by calculating the backward GF numerically. Next the quantity $J(r, z)$ is plotted around SHRU 1 to find a focus. We model the bottom as a uniform fluid halfspace and search for the bottom parameters that minimize the displacement of main focus from the virtual sound source. In the geoacoustic inversion, the searching region for bottom sound speed is from 1650 to 1900 m/s. For a given sound speed c_b, the corresponding density ρ_b is obtained by the Hamilton sediment empirical relationship for continental terrace[21]

$$c_\mathrm{b} = 2330.4 - 1257.0\rho_\mathrm{b} + 487.7\rho_\mathrm{b}^2. \tag{4}$$

Figure 4 gives the displacements of main focus from the virtual sound source SHRU 1, which are caused by deviations of bottom parameters from their true values. The minimum appears at the sound speed of 1770 m/s, which is the optimal value for the environment between SHRU 1 and SHRU 2. The optimal density is 2.0 g/cm^3 according to the empirical relationship of Eq. (4).

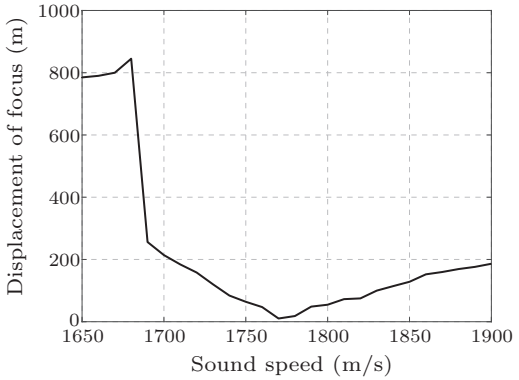

Fig. 4. Displacement of main focus from the virtual sound source versus bottom sound speed.

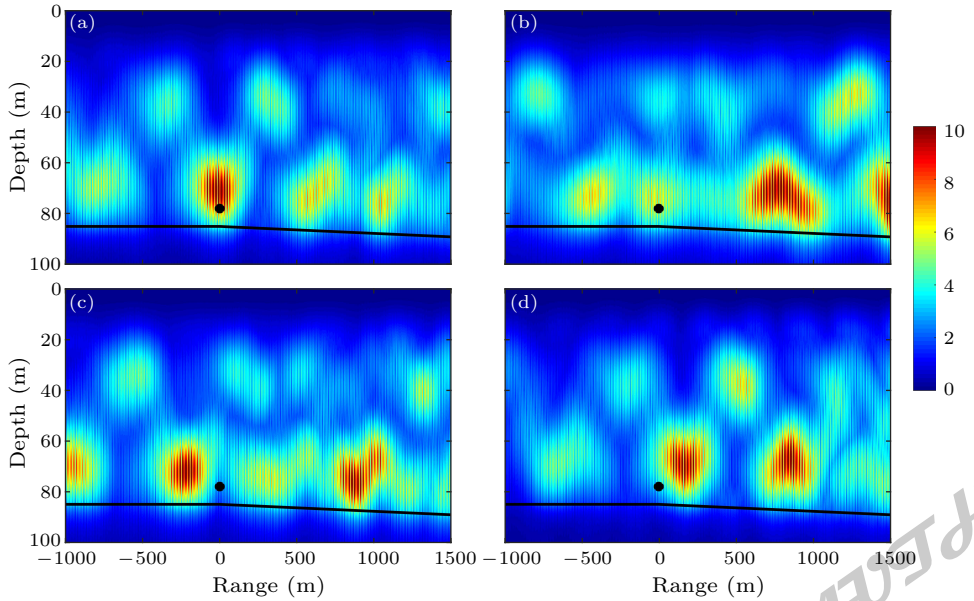

Fig. 5. Time reversal of GF retrieved from NCCF in the SW06 experiment. The GF is back-propagated in the environments with different bottom parameters. Normalized peak intensity of the back-propagated acoustic field in the vertical cross-section of the waveguide is shown by color. Sound speed and density in the bottom are (a) 1770 m/s and 2.0 g/cm^3, (b) 1650 m/s and 1.8 g/cm^3, (c) 1700 m/s and 1.9 g/cm^3, and (d) 1900 m/s and 2.2 g/cm^3. In each panel, the black dot denotes the position of the virtual sound source SHRU 1, and the bathymetry is indicated by a thick black line.

The normalized peak intensity $J(r, z)$ of the back-propagated field for the optimal bottom parameters is shown in Fig. 5(a). Remarkably, back propagation of the measured NCCF from the location of SHRU 2 gives a field with a pronounced focus in the vicinity of SHRU 1. The focusing quality of time-reversed NCCF in the experiment is comparable to that achieved in back-propagation of the simulated GF (Fig. 2(a)). The normalized peak intensity of the back-propagated field for other bottom parameters are also given in Figs. 5(b)–5(d). As in numerical simulations, the position of the main focus of the back-propagated NCCF proves to be sensitive to the bottom parameters. A mismatch between the actual bottom parameters and the parameters assumed in back-propagating the retrieved GF shifts and blurs the main focus, while making the spurious additional foci more pronounced. The corresponding bottom densities in Fig. 5 obtained from Eq. (4) are 2.0, 1.8, 1.9 and 2.2 $\mathrm{g/cm^3}$, respectively.

A uniform fluid halfspace bottom model is used in the inversion method, which includes three parameters: sound speed, density and attenuation. As discussed in Ref. [22], the equivalent single-layer bottom model has the same effect on the underwater acoustic field as the multiple-layer models within some range-frequency domain of interest. Furthermore, the Hamilton sediment empirical relationship between sound speed and density is utilized to reduce the dimension of unknown parameters. As a result, this inversion method could avoid the multiple-solution problem, which often appears in some other geoacoustic inversion methods. It should be emphasized that the inversion method combining NI and TRM techniques can also be applied to more complex bottom models. The additional parameters will lead to a considerable increase of computation time for searching optimal solutions, and the multiple-solution problem may appear.

In summary, a passive geoacoustic inversion method combining NI and TRM techniques has been presented, in which ambient noise recorded on only two hydrophones is used. In numerical simulations, strong focusing occurs in the vicinity of one hydrophone when the GF is back-propagated from the other hydrophone, with the position and strength of the focus being sensitive to sound speed and density in the bottom. We extract the GF from the NCCF measured by two single hydrophones in the SW06 experiment. After performing the TRM process, values of sound speed and density in the bottom are estimated by optimizing focusing of the back-propagated GF. Compared with active techniques, the passive inversion method does not contribute to noise pollution in the ocean, and consequently is inherently environmentally friendly. Moreover, this is a low-cost method because only two hydrophones are necessary.

References

[1] Fallat M R and Nielson P L 2000 *J. Acoust. Soc. Am.* **107** 1967
[2] Potty G R, Miller J H, Lynch J F and Smith K B 2000 *J. Acoust. Soc. Am.* **108** 973
[3] Dosso S E 2002 *J. Acoust. Soc. Am.* **111** 129
[4] Chapman N R, Chin-Bing S, King D and Evans R B 2003 *IEEE J. Oceanic Eng.* **28** 320
[5] Zhou J X, Zhang X Z, Rogers P H, Simmen J A, Dahl P H, Jin G L and Peng Z H 2004 *IEEE J. Oceanic Eng.* **29** 988
[6] Li F H and Zhang R H 2000 *Acta Acust.* **25** 298 (in Chinese)
[7] Li Z L and Li F H 2010 *Chin. J. Oceanol. Limnol.* **28** 990
[8] Guo X L, Yang K D, Ma Y L and Yang Q L 2015 *Chin. Phys. Lett.* **32** 124302
[9] Baggeroer A B, Kuperman W A and Mikhalevsky P N 1993 *IEEE J. Oceanic Eng.* **18** 401
[10] Siderius M, Harrison C H and Porter M B 2006 *J. Acoust. Soc. Am.* **120** 1315
[11] Lobkis O I and Weaver R L 2001 *J. Acoust. Soc. Am.* **110** 3011
[12] Wapenaar K 2004 *Phys. Rev. Lett.* **93** 254301
[13] Godin O A 2006 *Phys. Rev. Lett.* **97** 054301
[14] Godin O A 2009 *J. Acoust. Soc. Am.* **125** 1960
[15] Jackson D R and Dowling D R 1991 *J. Acoust. Soc. Am.* **89** 171
[16] Fink M, Cassereau D, Derode A, Prada C, Roux P, Tanter M, Thomas J L and Wu F 2000 *Rep. Prog. Phys.* **63** 1933
[17] Edelman G F, Akal T, Hodgkiss W S, Kim S, Kuperman W A and Song H C 2002 *IEEE J. Oceanic Eng.* **27** 602
[18] Roux P and Kuperman W A 2005 *J. Acoust. Soc. Am.* **117** 131
[19] Tang D J, Moum J N, Lynch J F, Abbot P, Chapman R, Dahl P H, Duda T F, Gawarkiewicz G, Glenn S, Goff J A, Graber H, Kemp J, Maffei A, Nash J D and Newhall A E 2007 *Oceanography* **20** 156
[20] Collins M D *User's Guide for RAM Versions 1. 0 and 1.0p* (Washington DC: Naval Research Laboratory)
[21] Hamilton E L and Bachman R T 1982 *J. Acoust. Soc. Am.* **72** 1891
[22] Li Z L and Zhang R H 2004 *Chin. Phys. Lett.* **21** 1100

Chinese Physics Letters

Volume 34 Number 9 September 2017

GENERAL

090101 Discovery of Fractionalized Neutral Spin-1/2 Excitation of Topological Order Views & Comments
Xiao-Gang Wen

090201 Soliton Solutions to the Coupled Gerdjikov–Ivanov Equation with Rogue-Wave-Like Phenomena
Jian-Bing Zhang, Ying-Yin Gongye, Shou-Ting Chen

090202 A Multi-Symplectic Compact Method for the Two-Component Camassa–Holm Equation with Singular Solutions
Xiang Li, Xu Qian, Bo-Ya Zhang, Song-He Song

090301 Sound Wave of Spin–Orbit Coupled Bose–Einstein Condensates in Optical Lattice
Xu-Dan Chai, Zi-Fa Yu, Ai-Xia Zhang, Ju-Kui Xue

090302 Space-to-Ground Quantum Key Distribution Using a Small-Sized Payload on Tiangong-2 Space Lab Express Letter
Sheng-Kai Liao, Jin Lin, Ji-Gang Ren, Wei-Yue Liu, Jia Qiang, Juan Yin, Yang Li, Qi Shen, Liang Zhang, Xue-Feng Liang, Hai-Lin Yong, Feng-Zhi Li, Ya-Yun Yin, Yuan Cao, Wen-Qi Cai, Wen-Zhuo Zhang, Jian-Jun Jia, Jin-Cai Wu, Xiao-Wen Chen, Shan-Cong Zhang, Xiao-Jun Jiang, Jian-Feng Wang, Yong-Mei Huang, Qiang Wang, Lu Ma, Li Li, Ge-Sheng Pan, Qiang Zhang, Yu-Ao Chen, Chao-Yang Lu, Nai-Le Liu, Xiongfeng Ma, Rong Shu, Cheng-Zhi Peng, Jian-Yu Wang, Jian-Wei Pan

090401 Effects of Homogeneous Plasma on Strong Gravitational Lensing of Kerr Black Holes
Chang-Qing Liu, Chi-Kun Ding, Ji-Liang Jing

090601 Direct Digital Frequency Control Based on the Phase Step Change Characteristic between Signals
Zhao-Min Jia, Xu-Hai Yang, Bao-Qi Sun, Xiao-Ping Zhou, Bo Xiang, Xin-Yu Dou

090602 Transportable 1555-nm Ultra-Stable Laser with Sub-0.185-Hz Linewidth
Zhao-Yang Tai, Lu-Lu Yan, Yan-Yan Zhang, Xiao-Fei Zhang, Wen-Ge Guo, Shou-Gang Zhang, Hai-Feng Jiang

090701 Terahertz Direct Detectors Based on Superconducting Hot Electron Bolometers with Microwave Biasing
Shou-Lu Jiang, Xian-Feng Li, Run-Feng Su, Xiao-Qing Jia, Xue-Cou Tu, Lin Kang, Biao-Bing Jin, Wei-Wei Xu, Jian Chen, Pei-Heng Wu

NUCLEAR PHYSICS

092101 Collective Flows of $^{16}O+^{16}O$ Collisions with α-Clustering Configurations
Chen-Chen Guo, Wan-Bing He, Yu-Gang Ma

FUNDAMENTAL AREAS OF PHENOMENOLOGY(INCLUDING APPLICATIONS)

094101 Effects of Breaking Waves on Composite Backscattering from Ship-Ocean Scene
Jin-Xing Li, Min Zhang, Peng-Bo Wei

094201 High-Order-Harmonic Generation from a Relativistic Circularly Polarized Laser Interacting with Over-Dense Plasma Grating
Xia-Zhi Li, Hong-Bin Zhuo, De-Bin Zou, Shi-Jie Zhang, Hong-Yu Zhou, Na Zhao, Yue Lang, De-Yao Yu

094202 Cadmium Selenide Polymer Microfiber Saturable Absorber for Q-Switched Fiber Laser Applications
A. H. A. Rosol, H. A. Rahman, E. I. Ismail, N. Irawati, Z. Jusoh, A. A. Latiff, S. W. Harun

094203 Leaky Modes in Ag Nanowire over Substrate Configuration
Yin-Xing Ding, Lu-Lu Wang, Li Yu

094301 Geoacoustic Inversion Using Time Reversal of Ocean Noise
Ji-Xing Qin, Boris Katsnelson, Oleg Godin, Zheng-Lin Li

PHYSICS OF GASES, PLASMAS, AND ELECTRIC DISCHARGES

095201 Heat Flux on EAST Divertor Plate in H-mode with LHCD/LHCD+NBI
Bo Shi, Zhen-Dong Yang, Bin Zhang, Cheng Yang, Kai-Fu Gan, Mei-Wen Chen, Jin-Hong Yang, Hui Zhang, Jun-Li Qi, Xian-Zu Gong, Xiao-Dong Zhang, Wei-Hua Wang

CONDENSED MATTER: STRUCTURE, MECHANICAL AND THERMAL PROPERTIES

096101 A Bright Single-Photon Source from Nitrogen-Vacancy Centers in Diamond Nanowires
Shen Li, Cui-Hong Li, Bo-Wen Zhao, Yang Dong, Cong-Cong Li, Xiang-Dong Chen, Ya-Song Ge, Fang-Wen Sun

096201 New Insights on the Deflection and Internal Forces of a Bending Nanobeam
De-Min Zhao, Jian-Lin Liu

096801 Fluorescence Enhancement of Metal-Capped Perovskite $CH_3NH_3PbI_3$ Thin Films
Peng Sun, Wei-Wei Yu, Xiao-Hang Pan, Wei Wei, Yan Sun, Ning-Yi Yuan, Jian-Ning Ding, Wen-Chao Zhao, Xin Chen, Ning Dai

CONDENSED MATTER: ELECTRONIC STRUCTURE, ELECTRICAL, MAGNETIC, AND OPTICAL PROPERTIES

097301 Characterization of Interface State Density of Ni/p-GaN Structures by Capacitance/Conductance-Voltage-Frequency Measurements
Zhi-Fu Zhu, He-Qiu Zhang, Hong-Wei Liang, Xin-Cun Peng, Ji-Jun Zou, Bin Tang, Guo-Tong Du

097302 Fast Electrical Detection of Carcinoembryonic Antigen Based on AlGaN/GaN High Electron Mobility Transistor Aptasensor
Xiang-Mi Zhan, Quan Wang, Kun Wang, Wei Li, Hong-Ling Xiao, Chun Feng, Li-Juan Jiang, Cui-Mei Wang, Xiao-Liang Wang, Zhan-Guo Wang

097303 Fano Resonance Effect in CO-Adsorbed Zigzag Graphene Nanoribbons
Gao Wang, Meng-Qiu Long, Dan Zhang

097304 Improved Operation Characteristics for Nonvolatile Charge-Trapping Memory Capacitors with High-κ Dielectrics and SiGe Epitaxial Substrates
Zhao-Zhao Hou, Gui-Lei Wang, Jin-Juan Xiang, Jia-Xin Yao, Zhen-Hua Wu, Qing-Zhu Zhang, Hua-Xiang Yin

097305 Evidence of Electron-Hole Imbalance in WTe_2 from High-Resolution Angle-Resolved Photoemission Spectroscopy
Chen-Lu Wang, Yan Zhang, Jian-Wei Huang, Guo-Dong Liu, Ai-Ji Liang, Yu-Xiao Zhang, Bing Shen, Jing Liu, Cheng Hu, Ying Ding, De-Fa Liu, Yong Hu, Shao-Long He, Lin Zhao, Li Yu, Jin Hu, Jiang Wei, Zhi-Qiang Mao, You-Guo Shi, Xiao-Wen Jia, Feng-Feng Zhang, Shen-Jin Zhang, Feng Yang, Zhi-Min Wang, Qin-Jun Peng, Zu-Yan Xu, Chuang-Tian Chen, Xing-Jiang Zhou

097701 Origin of Negative Imaginary Part of Effective Permittivity of Passive Materials
Kai-Lun Zhang, Zhi-Ling Hou, Ling-Bao Kong, Hui-Min Fang, Ke-Tao Zhan

097801 Effect of Droop Phenomenon in InGaN/GaN Blue Laser Diodes on Threshold Current
Xiao-Wang Fan, Jian-Ping Liu, Feng Zhang, Masao Ikeda, De-Yao Li, Shu-Ming Zhang, Li-Qun Zhang, Ai-Qin Tian, Peng-Yan Wen, Guo-Hong Ma, Hui Yang

CROSS-DISCIPLINARY PHYSICS AND RELATED AREAS OF SCIENCE AND TECHNOLOGY

098101 Nonresonant and Resonant Nonlinear Absorption of CdSe-Based Nanoplatelets
Li-Bo Fang, Wei Pan, Si-Hua Zhong, Wen-Zhong Shen

098701 Temperature Impacts on Transient Receptor Potential Channel Mediated Calcium Oscillations in Astrocytes
Yu-Hong Zhang, Hui Liu, Ying-Rong Han, Ya-Fei Chen, Su-Hua Zhang, Yong Zhan